Macromolecules

ARTICLE

pubs.acs.org/Macromolecules

Controlling Nanorod Self-Assembly in Polymer Thin Films

Miguel A. Modestino,[†,‡] Elaine R. Chan,[§] Alexander Hexemer,[§] Jeffrey J. Urban,[⊥] and Rachel A. Segalman*[,†,‡]

[†]Department of Chemical and Biomolecular Engineering, University of California, Berkeley, California 94720, United States

[‡]Materials Science Division, Lawrence Berkeley National Laboratory, Berkeley, California 94720, United States

[§]Advanced Light Source, Lawrence Berkeley National Laboratory, Berkeley, California 94720, United States

[⊥]The Molecular Foundry, Lawrence Berkeley National Laboratory, Berkeley, California 94720, United States

Supporting Information

ABSTRACT: The integration of functional polymers and semiconducting nanorods can lead to properties unattainable by either of the components independently. Elongated nanocrystals provide advantageous anisotropic physical properties which could be uniquely harnessed via integration into hybrid materials, if control over their orientation could be imposed. Controlling this orientation of anisotropic nanocrystals in polymer composites is challenging due to the presence of multiple interactions between the nanorods, polymer, and surfaces of the films. This study demonstrates a simple yet versatile method to obtain vertically aligned nanorod arrays in polymer composites over large areas. Comparison of systems consisting of rods of varying geometry and chemistry of ligand and/or polymer indicates that nanorod−nanorod interactions dominate the self-assembly behavior of the nanocrystals, while weak polymer−nanorod interactions can lead to independent co-self-assembly of each of the components in the system and allow for the incorporation of a wide variety of polymers with complementary functionality. Aligned nanorod composites can provide fundamental understanding of both the phase behavior and anisotropic electronic properties of nanorods in polymers. Incorporating functional polymers can enable the fabrication of efficient hybrid thin film devices for applications in photovoltaics, LEDs, and solar-fuel membranes.

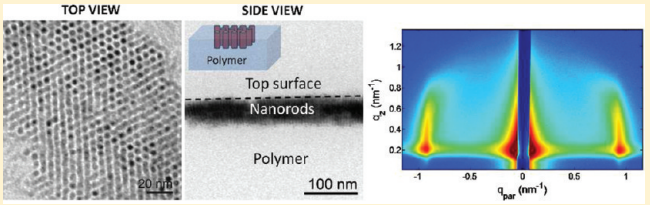

INTRODUCTION

Polymer−semiconductor nanoparticle composites offer the promise of efficient and inexpensive solution-processable optoelectronics. In particular, colloidal nanorods have been suggested as building blocks for photovoltaic,[1] light-emitting,[2,3] and solar-fuel devices.[4] The electronic properties of these materials are tunable through chemistry, size, and shape. For example, when the shape symmetry of the nanoparticles is broken, the properties become anisotropic. Cadmium chalcogenide rods show polarized electro- and photoluminescence along their long axis;[5,6] hybrid nanorods can localize charge on separated regions of their structure,[7,8] and photocatalytic nanorods can carry out redox reactions in distinct locations of the nanocrystals.[4] In order to incorporate anisotropic nanocrystals into functional hybrid devices, it is crucial to achieve large-scale orientational order of these systems, which remains a significant challenge. If achieved, orientational control of nanorods in polymer composites could enable nanocrystal properties to act collectively to maximize device performance.

Several groups have shown small scale alignment of colloidal nanorods in the past, both by the use of external electrical fields,[9,10] controlled evaporation techniques,[11−13] and addition of depleting agents to nanorod solutions[14] or by tuning the solubility properties of amphiphilic nanorods.[15] More recently, Baker et al. have demonstrated the achievement of device-scale vertical alignment of CdS nanorods by carefully controlling the evaporation rate of the solvent from nanorod solutions.[16] While aligned nanorod arrays represent a viable solution-processable alternative for the fabrication of crystalline semiconductor thin film devices, a functional polymer matrix provides advantages for optoelectronic applications. A previous study by Gupta et al. demonstrated that the use of large electric fields could lead to vertically oriented nanorod arrays embedded in a polymer matrix.[9] In general, polymers can add structural stability and complementary properties such as improved light absorption to thin films composed entirely of nanorods. Understanding of the self-assembly factors that lead to aligned arrays of anisotropic nanocrystals in polymer composites can lead to the fabrication of nanostructured hybrid materials over large areas.

This work provides insights on the role of nanorod and polymer interactions in the self-assembly behavior of anisotropic nanocrystals in composites. We demonstrate that control over the interactions between nanorod surfaces can result into different self-assembly behavior and ultimately lead to vertical orientation of colloidal CdSe nanorods in composite thin films over areas larger than 1 cm^2. Composite systems with strong rod−rod interactions result in aligned arrays of nanorods independently of the chemical nature of the polymer matrix, which

Received: June 3, 2011
Revised: August 18, 2011
Published: September 06, 2011

conveniently allow for the fabrication of composites with a wide variety of polymer functionalities. As part of this study, grazing-incidence small-angle scattering (GISAXS) was used to investigate the long-range order of the system and gain insights into the nanorod self-assembly mechanism.

EXPERIMENTAL SECTION

Materials. Cadmium oxide (CdO), trioctylphosphine oxide (TOPO) (90% purity, Batch MKAA3064), trioctylphosphine (TOP), tributylphosphine (TBP), 11-mercaptoundenoic acid (MUA), selenium (Se), polyvinylcarbazole (PVK) (M_n = 25 000−50 000 g/mol), 1,2-dichlorobenzene (DCB), and Nafion 5% solution were obtained from Sigma-Aldrich. Dodecylphosphonic acid (DDPA), tetradecylphosphonic acid (TDPA), hexadecylphosphonic acid (HDPA), and octadecylphosphonic acid (ODPA) were obtained from PCI Synthesis. Poly(3-hexylthiophene) (M_n = 50 000 g/mol) was obtained from Rieke Metals, Inc. Polystyrene samples of various molecular weights (M_n = 3500 g/mol, M_w/M_n = 1.06; M_n = 52 000 g/mol, M_w/M_n = 1.07; M_n = 400 000 g/mol, M_w/M_n = 1.06; M_n = 1 000 000 g/mol, M_w/M_n = 1.03), poly(styrene-*b*-ethylene oxide) (M_n = 20 000 g/mol (PS):6500 g/mol (PEO), M_w/M_n = 1.06), and poly(2-vinylpyridine) (M_n = 50 000, M_w/M_n = 1.04) were obtained from Polymer Source.

CdSe Nanorod Preparation. Alkyl-passivated CdSe nanorods were synthesized following methods previously reported in the literature.[17] A typical synthesis involved complexation of CdO (1.6 mmol, 0.2054 g) with TDPA (3.2 mmol, 0.8928 g) in 3 g of TOPO. This solution was heated up to 350 °C under an inert atmosphere to form the cadmium precursor. When the solution became transparent, the temperature was lowered to 150 °C and kept under vacuum for 40 min. The solution was then heated under nitrogen to 300 °C, and a solution containing 0.53 mL of a 1 M TOP-Se solution, 0.126 g of TBP, and 0.73 g of TOP was quickly injected. The CdSe rods were allowed to grow for 15 min at 250 °C, and the reaction was quenched by rapidly decreasing the temperature to room temperature. The resulting rods were washed by dispersing them in toluene and precipitating with methanol (MeOH), redissolving them in a mixture of 2:1 chloroform: octylamine, precipitating them with MeOH again, and then redispersing in hexanes and precipitating with MeOH once more. After these cleaning steps, the rods were kept in chloroform solutions with concentrations of ∼10 mg/mL. This procedure resulted in CdSe nanorods with approximate dimensions of 30 × 4 nm.

Pyridine ligand exchange was performed by refluxing the nanorods under nitrogen in pyridine for 24 h. For the 11-mercaptoundenoic acid (MUA) ligand exchange, 10 mg of CdSe was dissolved in 15 mL of chloroform along with 20 mg of MUA, and the solution was refluxed at 65 °C for 24 h. Following the exchange reaction, 3 mL of a 1% m/v water solution of tetramethylammonium hydroxide was added, and the CdSe rods were extracted in the aqueous phase.

Thin Film Casting and Characterization. Polymer−nanorod composites were obtained by drop-casting under controlled evaporation conditions. An in-house built solvent annealing chamber was used to control the casting temperatures and solvent vapor saturation conditions. All films were cast on silicon substrates coated with a 50 nm layer of poly(3,4-ethylenedioxythiophene):poly(styrenesulfonate) (PEDOT:PSS). Solutions of nanorods and polymers in 1,2-dichlorobenzene (DCB) were drop-cast inside the controlled environment chamber with a nitrogen atmosphere partially saturated with DCB and maintaining a constant substrate temperature of 45 °C. The casting solutions consisted of 1−3 mg/mL of polymer and 0.5−2 mg/mL of CdSe rod solution in DCB, and the concentration of CdSe was determined by drying and weighting a known amount of solution. For MUA covered rods, dimethyl sulfoxide (DMSO) was used as the casting solvent.

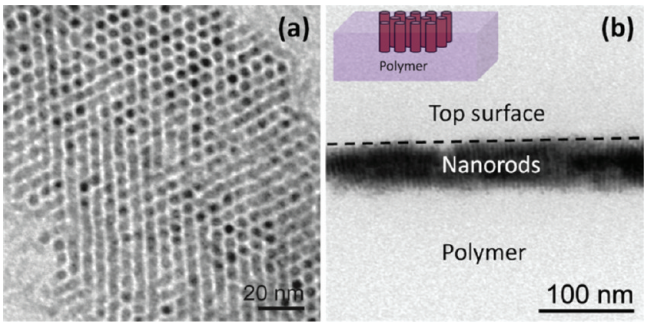

Figure 1. (a) Transmission TEM images of the films show CdSe nanorods self-assembling in vertically aligned arrays dispersed in a polystyrene. The cross-sectional TEM view of a P3HT/CdSe composite in (b) reveals segregation of nanorods toward the film surfaces.

The composite films were characterized by transmission electron microscopy (TEM), atomic force microscopy (AFM), and grazing-incidence small-angle X-ray scattering (GISAXS). TEM samples were prepared by floating films in water onto copper grids and imaged using a FEI Tecnai microscope. Cross-sectional TEM samples were obtained by embedding films in epoxy resin and using a microtome to obtain ∼100 nm thick cross-sectional samples of the composite films. AFM images were obtained using a Veeco Multimode SPM in tapping mode. GISAXS patterns were obtained at beamline 7.3.3 of the Advanced Light Source at Lawrence Berkeley National Laboratory.[18] The X-ray wavelength used was λ = 0.124 nm, with a monochromator energy resolution of E/dE of 100. For all the experiments performed, the sample-to-detector distance was set at ∼2 m, and 2-D scattering patterns were collected with an ADSC CCD Camera Quantum 4 (pixel size 81.7 μm).

RESULTS AND DISCUSSION

Thin Film Self-Assembly Behavior. Drop-casting thin films from low vapor pressure solvents (such as DCB) and inside a saturated solvent atmosphere allows for a slow evaporation process in which the nanorods can self-assemble prior to becoming trapped in the polymer film. Following this slow evaporation technique, self-assembled composites with vertically aligned arrays of alkyl-passivated nanorods can be obtained as observed in the TEM images in Figure 1. Multiple interactions can play a role in the self-assembly of nanorods in these systems. van der Waals (VdW) interactions between the nanorods, the polymer chains and the substrate, and air interfaces all have an effect in the self-assembly behavior of each component. Although CdSe crystals have a permanent dipole moment, the dipole−dipole coupling interactions between nanocrystals are small when compared with the VdW interactions between alkyl-passivated nanorods.[16,19] The presence of strong rod−rod interactions and polymer mediated depletion attraction interactions will favor the formation of hexagonal nanorod arrays that macrophase separate from the polymer containing solution[14] and when confined to a thin film morphology can lead to uniaxial alignment of the nanorods within the films. This solution self-assembly process prior to complete solvent evaporation is evident from solution small-angle X-ray scattering (SAXS) patterns that demonstrate the formation of hexagonally packed arrays of rods in concentrated solutions (see Supporting Information, Figure S1). Additionally, surface energy and entropic effects can result in segregation of the nanocrystals arrays to the interfaces of the films at a later stage of the casting process.[20,21] These surface effects are observed in the cross-sectional TEM image presented

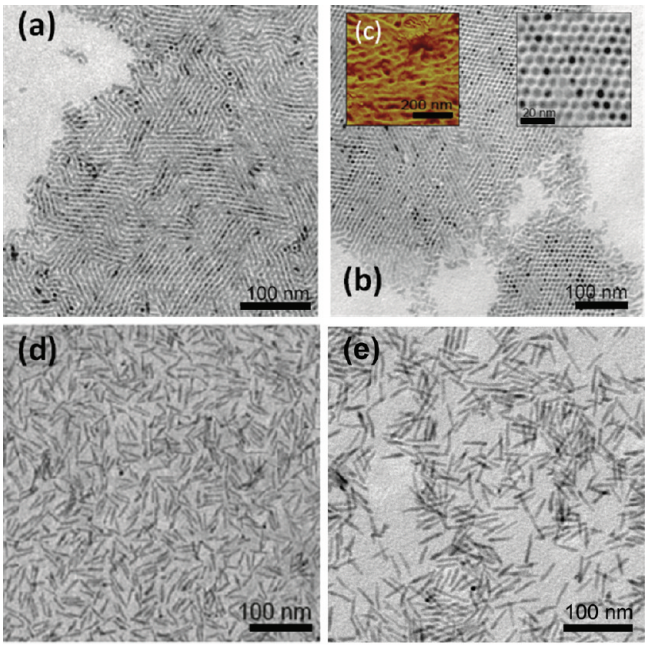

Figure 2. TEM images indicate the presence of equivalent arrays in composites with a PVK matrix in (a) as well as a P3HT matrix in (b). The AFM image in (c) shows the fibrillar structure of P3HT at the surface of the composites. Passivating ligands such as (d) pyridine and (e) MUA prevent the formation of ordered rod arrays.

in Figure 1b, where nanorod arrays are located preferentially at the air−polymer interface of the composite. The segregation of nanorod arrays to the surface of thin films can further aid the alignment of nanorods in the composites as they are confined to a two-dimensional space.

Remarkably, the results presented above appear to be qualitatively consistent over a wide variety of polymer matrixes, independent of the specific chemistry or physical properties of the polymer. Oriented nanorod arrays were obtained in electronically active polymers with potential optoelectronic applications such as PVK and P3HT.[1,22] Glassy and hydrophobic polymers such as PS have an equivalent effect on arrays as well as more polar systems like P2VP. Degradable polymers such as PLA also allow for the formation of vertically aligned arrays of nanorod. This type of matrix can be conveniently used for the development of simple transfer methods of oriented rod arrays into different substrates and configurations.

As an example, TEM images of nanorod arrays in PVK and P3HT are presented in Figure 2. The AFM phase image presented in Figure 2c exposes the irregular fibrillar structure at the surface of a P3HT composite. Regardless of the polymer morphology, vertically aligned arrays are formed throughout the film. Our observations suggest that polymer−rod interactions are weak in the case of alkyl-passivated nanorods, thereby allowing us to obtain similar results over a wide variety of systems. This is quite useful for the design of functional materials because the nanorod and polymer systems can be tuned easily without significant effects in morphology. A drastic change in the self-assembly behavior is evidenced when the passivation of the nanorods is modified with chemically dissimilar ligands. Figures 2d and 2e present results from composite films containing pyridine and MUA exchanged nanorods in a P3HT and Nafion matrices, respectively. The TEM micrographs for these composites show nanorods isotropically dispersed within the polymer matrix. In the cases described above, chemical changes in the surface passivation of the nanorods can increase the miscibility of the nanocrystals in the polymer composites. Additionally for pyridine exchanged nanorods, the effective excluded volume of the nanorods is reduced when compared to alkyl-passivated rods; this decrease in excluded volume will reduce the region for depletion interactions to occur and result in dispersion of the rods in the polymer matrix. For MUA passivated rods, electrostatic repulsion between charged carboxylic groups can also prevent the formation of arrays. The factors discussed above can ultimately result in the dispersion of nanorods observed in the system.

Understanding the nanorod self-assembly mechanism can lead to the development of more efficient and uniform casting methods as well as control over the nanorod array dimensions. The use of polymers in combination with semiconducting nanorods not only leads to new and improved functional materials but also can aid the nanorod self-assembly by triggering depletion−attraction interactions that can lead to macrophase separation of the system. Other groups have studied the effect of polymers as depleting agents on solution self-assembly of nanorods, resulting in the formation of hexagonal arrays.[14] These polymer-induced depletion−attraction interactions are consistent with the macrophase separation of the rods in the system, where the depletion of polymer chains from the inter-rod region results in entropic gains that generate a net attractive interaction between nanorods. On the other hand, these interactions do not provide a direct explanation for the strong dependence on the ligands on the self-assembly, which suggest that enthalpic interactions between nanorods are also important in the self-assembly process and are complementary to depletion interactions in the system.

While drastic variations in the chemical nature of the ligands have shown significant effects in the behavior of nanocrystals, varying the ligand interactions in a controlled, graduated manner can provide further insight into the role of rod−rod interactions on the self-assembly process. Progressively increasing the length of the passivating ligands will gradually change the interactions between nanorods. The effects of these changes are not significant enough to qualitatively alter the self-assembled structure when the length of the alkyl chains ranges from 12 to 18 carbons, though it is clear that such changes have a significant effect on inter-rod interactions and can affect the detailed long-range order. As proof, Figure 3a shows that all of these experimentally accessible systems self-assemble into qualitatively equivalent vertically aligned arrays. Close observation of the nanorod arrays, however, indicates that the system has a high degree of local order, as evidenced by the sharp peaks that evolve from the pair number density distribution as a function (PDF) of inter-rod distance (Figure 3b). Furthermore, the positions of the peaks in the PDF and the fast Fourier transform (FFT) of the TEM image (shown in the inset of Figure 3b) are consistent with the passivated nanorods approaching hexagonal close-packing. This result provides further evidence of nanorods completely macrophase separating from the polymer matrix, in congruence with strong nanorod interactions dominating the self-assembly behavior of alkyl-coated nanorods.

GISAXS Analysis. The analysis presented above provides qualitative insights on the self-assembly process that leads to vertically aligned arrays in thin-film composites. To complement the observations previously presented, GISAXS patterns provide a quantitative description of the internal morphology of composites

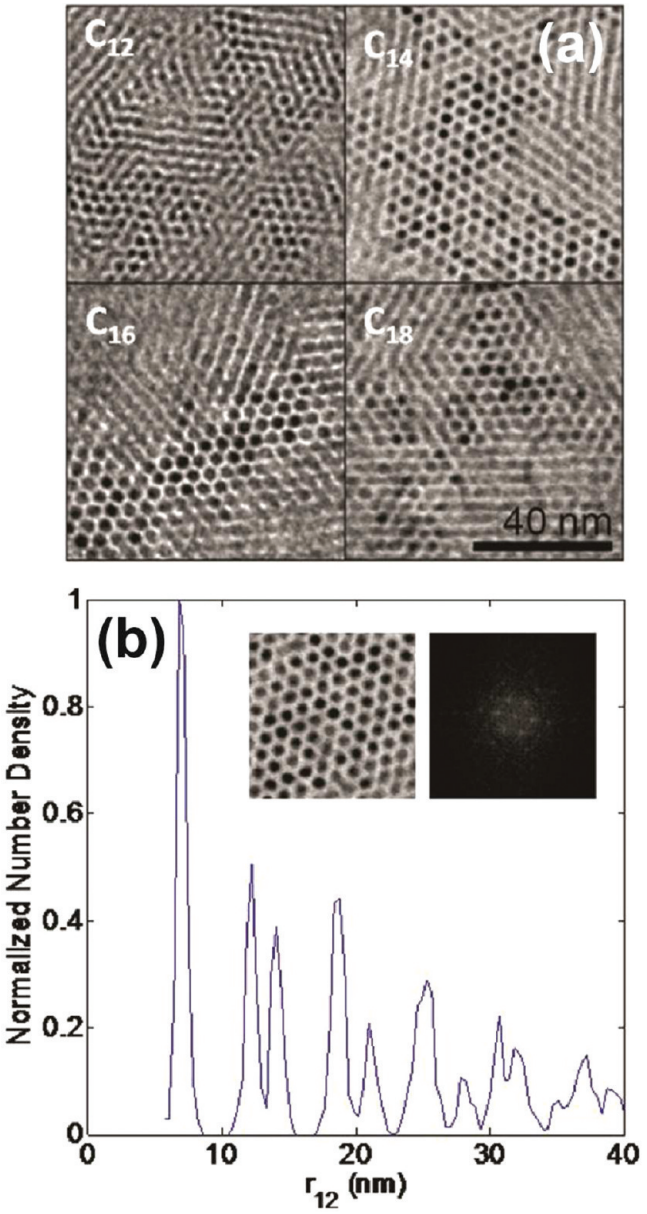

Figure 3. Nanorods with different degrees of passivation form similar hexagonal arrays in a polystyrene matrix as shown in the TEM images in (a). The sharp peaks in the pair number density distribution for TDPA passivated nanorods in (b) as well as the defined hexagonal structured observed in the FFT demonstrate that the system contains a high degree of local order.

and in this way help elucidate the effects of different factors in the nanorod self-assembly process. Analysis of GISAXS patterns for thin films is complex due to multiple scattering events that arise from beam reflections from the substrate. Commonly, these patterns are analyzed by adopting a distorted-wave Born approximation (DWBA) formalism to generate scattering models that can serve to quantitatively assess the morphology of nanostructured thin films.[23−26] Within the DWBA formalism, the scattering in the plane of the film is treated using a kinematic approximation (only single scattering events are considered), while a dynamic treatment is given for the out-of-plane scattering that accounts for multiple scattering events. Contributions from each of the scattering events are weighted by the reflection and transmission coefficient of each of the layers in the system. The selection of the incident and scattered vectors was carried out following similar GISAXS analysis performed on polymer samples.[24]

Figure 4 presents a schematic representation the grazing incidence geometry as well as of the scattered vectors in the normal direction, $q_{z,i}$, for each of the scattering events present in grazing incidence scattering experiments. They are calculated from the normal components of the incident and diffracted waves, $k_{i,z}$ and $k_{i,f}$. The parallel component of the scattering vector, q_{par}, is calculated as $q_{par} = (q_x^2 + q_y^2)^{1/2}$. In this way, the scattering intensity can be written as

$$I = \frac{1}{16\pi^2}[T_i T_f F(q_{par}, q_{z,1}) + T_i R_f F(q_{par}, q_{z,2}) + T_f R_i F(q_{par}, q_{z,3}) + R_i R_f F(q_{par}, q_{z,4})]^2 \quad (1)$$

where T_i, T_f, and R_i, R_f account for the intensity of the transmitted and reflected waves associated with the incident (i) and diffracted beam (f), respectively, and were calculated using Parrat relations.[24,27] The scattering potential, $F(q_{par},q_{z,i})$, is calculated as the product of the form factor $P(q_{par},q_z)$, which includes information regarding the shape of the object, the structure factor $S(q)$, resulting from the position of the scattering objects inside the unit cell, and the geometric structure factors $G(q)$ corresponding to the position of the unit cells within a lattice.

Based on TEM observations, the composite morphology for the scattering model has been defined as arrays of nanorods hexagonally packed and segregated to the top surface of composites. X-ray scattering patterns have been generated for a range of arrays with different rod tilt angles, ϕ, as depicted in Figure 5a. For the scattering system in consideration, the nanorod form factor can be calculated assuming a cylindrical shape for the nanorods.[28] The scheme presented in Figure 5b details the geometry used in this calculation where α is the angle between the scattering vector q and the axis of the rods, and θ is the angle of the in-plane projection of the rod. Given that nanorods with a tilt angle φ can attain any in-plane orientation, θ, it is necessary to average over all this configurations to calculate the overall 2D pattern arising from a sample. In the calculations presented in this study, the following equations were used to estimate the form factor arising from nanorods at different tilt angles

$$q_{par} = |\boldsymbol{q}| \sin\alpha \quad (2)$$

$$q_z = |\boldsymbol{q}| \cos\alpha \quad (3)$$

$$f(q,\phi,\theta) = 2V_{cyl}\frac{\sin\left(\frac{q_z L}{2}\right)}{\frac{q_z L}{2}}\frac{J_1(q_{par}R)}{q_{par}\sin\alpha}e^{-iq_z L/2} \quad (4)$$

$$P(q,\phi) = \frac{1}{2\pi}\int_0^{2\pi} f(q,\phi,\theta)\,d\theta \quad (5)$$

where L and R are the length and radius of the nanorods, respectively, and V_{cyl} is the volume of the nanorods. These values were estimated from TEM observations. To calculate the contribution from the structure and geometric factor, a 2D hexagonal close packing (HCP) of the nanocrystals was assumed, with lattice vectors a_1 and a_2 as represented in Figure 5c. The lattice

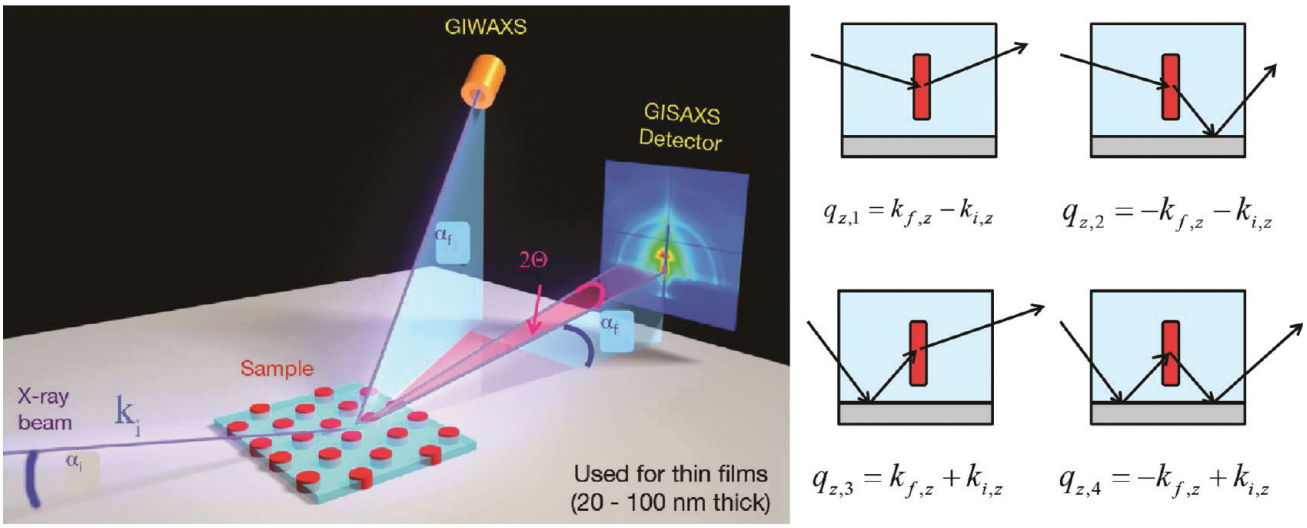

Figure 4. Representation of grazing incidence X-ray scattering experiment geometry and multiple scattering events present in GISAXS experiments.

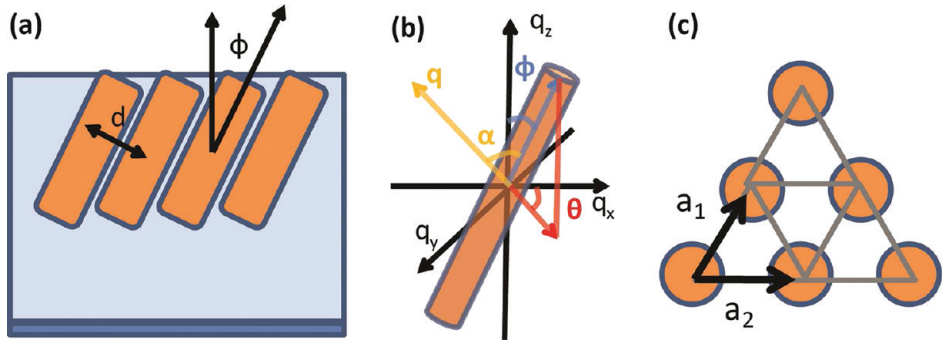

Figure 5. (a) Definition of model system used in GISAXS model, (b) coordinates used in the scattering calculations, and (c) lattice vectors for a 2-dimensional hexagonally close-packed structure.

vectors were estimated from the q_{par} position of the first Bragg peak in the experimental scattering profiles. In 2D, the HCP unit cell only contains one nanorod resulting in a structure factor equal to 1 while the geometric factor is dependent on the lattice vectors of the assembly and is calculated as

$$G(q) = \sum_{n_1=-\infty}^{+\infty} e^{i(n_1 \mathbf{q}\cdot\mathbf{a}_1)} \sum_{n_2=-\infty}^{+\infty} e^{i(n_2 \mathbf{q}\cdot\mathbf{a}_2)} \quad (6)$$

For all the quantitative analysis performed in this study, only the primary scattering peak arising from the nanorod arrays was considered, due to low intensity of the higher order peaks from the experimental data. Also, the calculated patterns were convoluted with the beamline resolution.

Nanorod tilting will result in asymmetries in the magnitude of the lattice vectors a_1 and a_2, which in turn will cause the splitting of the Bragg reflections into two scattering peaks or a peak broadening at small tilt angles. In the GISAXS patterns analyzed in this study no peak splitting has been observed, which suggests a small nanorod tilt angle that produces a negligible difference in the scattering position (see Supporting Information, Figure S2). Based on this observation, the magnitude of the lattice vectors a_1 and a_2 are set to be equivalent in the scattering calculations. A more significant effect in the peak shape can arise from variations in the inter-rod spacing in the arrays. From the PDF obtained from TEM images, the standard deviation of the closest inter-rod distance was calculated to be 8.5% of the mean interparticle separation; these spacing variations can cause a significant broadening of the scattering peaks. Finally, effects due to the finite size of the lattice can contribute to the peak broadening and also were considered in the calculations performed in this study. To account for these effects, a Gaussian distribution for the magnitude of the inter-rod spacing was assumed, with a mean value estimated from the q_{par} position of the maximum intensity peak in the experimental scattering profiles. The standard deviation on these lattice parameters was determined to be 0.011 nm^{-1} by fitting the shape of the primary Bragg peak obtained from the model to the experimental profiles as a function of q_{par}. On the basis of the standard deviation of the inter-rod spacing obtained from TEM, these value was estimated to be 0.008 nm^{-1}, which is remarkably close to the value observed from the experimental GISAXS pattern. The small difference in peak broadening observed in the GISAXS patterns can be accounted by lattice size broadening. By performing a simple analysis following a Scherrer formalism, the mean lattice size is estimated to be 80 nm, also commensurate with TEM observations.[29] In Figure 6a, a line cut of the 2D experimental scattering profile passing through the maximum intensity peak is compared to the calculated profile. Given the direct correlation of the width in the q_{par} direction of the primary scattering peak to the degree of fluctuations in the

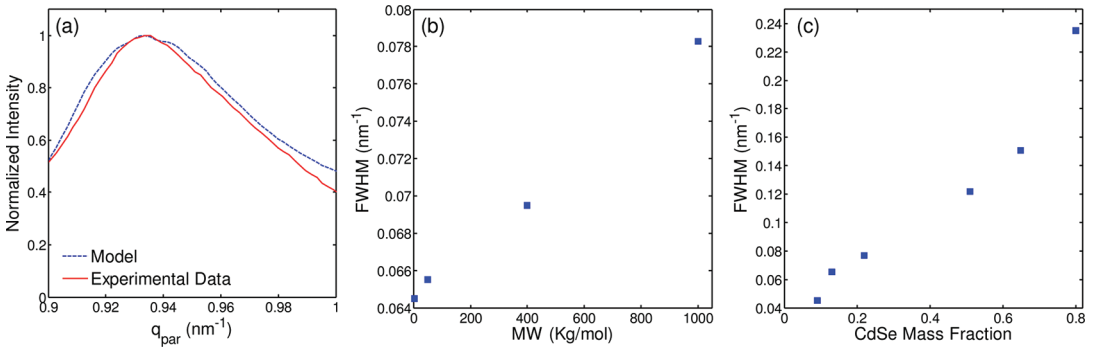

Figure 6. Incorporation of inter-rod spacing fluctuations results in modeled scattering profiles that match the experimental data as shown in (a). Kinetic effects increase inter-rod spacing fluctuations as evidenced from increasing peak broadening as a function of polymer molecular weight (b) and nanorod loading (c).

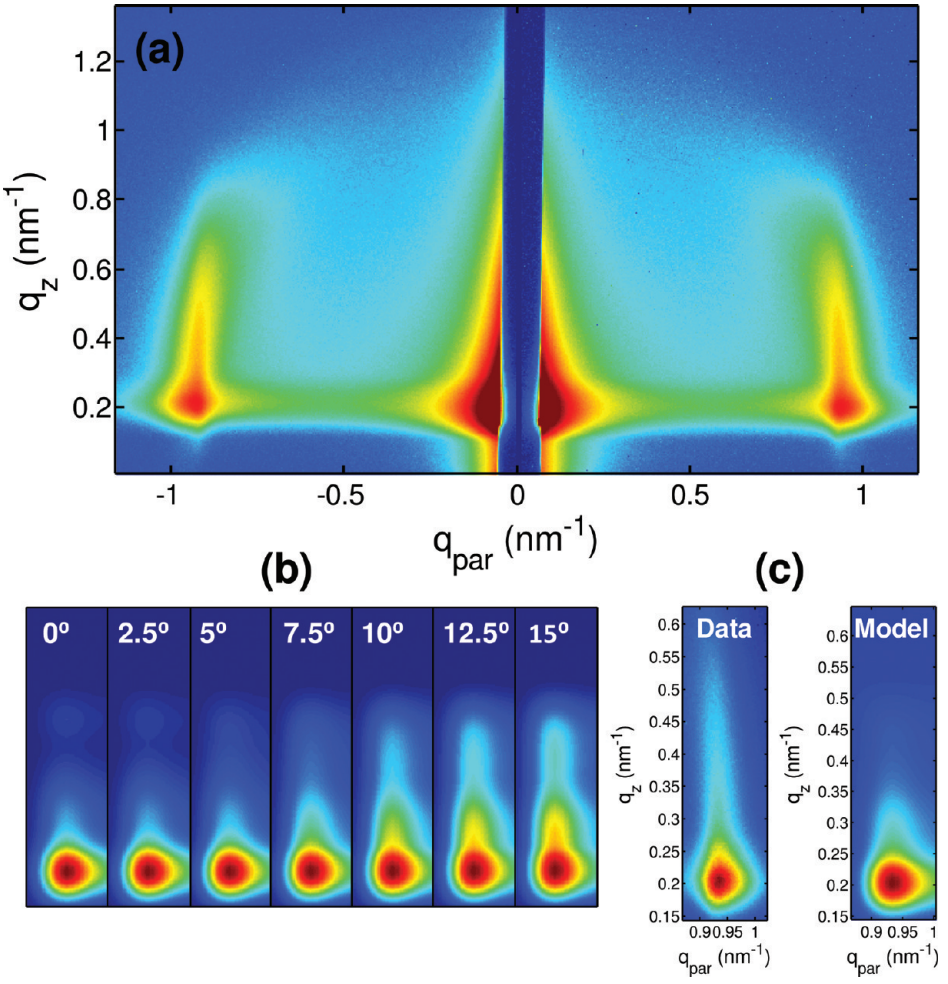

Figure 7. A representative GISAXS pattern obtained from a composite of CdSe nanorods in a PVK matrix is shown in (a). The modeled patterns obtained for composites with arrays presenting different tilt angles are presented in (b). Optimizing for the angle distribution function of the rods leads to optimized patterns that resemble the experimental data as shown in (c).

inter-rod spacing and lattice size, the level of order of the system can be evaluated directly from an analysis on the peak's broadening.

Analyzing the effect of different factors on long-range order of the composites can illuminate several aspects of the self-assembly process. Using the peak broadening as a gauge for the degree of order of the nanorod assemblies, Figure 6b,c presents the effects of polymer molecular weight and nanorod concentration in the self-assembly of composites. As evidenced in Figure 6b, by increasing the molecular weight of the polymer, a monotonic increase in the peak broadening is observed, indicating a decrease in the order of the system. Composites cast with high molecular weight polymers will lead to higher viscosity in the casting solution; this, in turn, will decrease the diffusion coefficients of the nanorods and can truncate the formation of ordered arrays at

dx.doi.org/10.1021/ma201252d |*Macromolecules* 2011, 44, 7364–7371

an earlier stage during the casting process. Moreover, analyzing the origin of the inter-rod spacing fluctuations, it is expected that for arrays of rods that macrophase separate from the polymer matrix, the level of these fluctuations will remain constant in the interior portion of the hexagonally packed arrays. A larger degree of spacing fluctuations is anticipated on the periphery of the arrays where nanorods are incorporating into the arrays. This indicates that a larger degree of spacing fluctuation can result from the presence of smaller arrays which would be expected for systems trapped at earlier stages during the casting process. The effect of nanorod concentration is also consistent with this observation. Composites cast from concentrated solutions of nanorods will not only result in a decrease in nanorod mobility at an earlier stage of drying but also will result in the presence of a larger number of nucleation centers for nanorod arrays which could reduce the overall size of the ordered arrays. This decrease in the long-range order of the system is evidenced by the increase in the primary peak broadening as presented in Figure 6c. The results described above demonstrate that kinetic effects are important in the growth of large arrays of nanorods in thin-film composites.

Furthermore, GISAXS patterns provide quantitative information regarding the orientation of nanorods in the composites; a typical GISAXS pattern from an alkyl-passivated nanorod composite is shown in Figure 7a. The model described above allows for the calculation of scattering patterns for arrays of nanorods with different tilt angles, ϕ, and uses these modeled patterns to extract information regarding the overall distribution of tilt angles in the composites (Figure 7b shows calculated patterns for various tilt angles). A Gaussian distribution function was used to describe the range of tilt angles, from which the average tilt angle, as well as standard deviation in tilt angle, was optimized. To find the optimal tilt angle distribution, the modeled pattern was constructed as the weighted average for the calculated patterns at different tilt angles. The modeled and experimental patterns were normalized with respect to the maximum intensity peak, and the q_z position of the peak for the modeled pattern was set equal to that of the experimental pattern. The fitting protocol minimized the square difference between then 2D modeled patterns and the obtained data. This analysis concluded that the average tilt angle that best describes our systems is below 10° with a standard deviation of less than 5°. An optimized pattern with mean tilt angle of 5° and standard deviation of 2° is compared with an experimental profile in Figure 7c. Consistent with the TEM observations, GISAXS data confirmed the presence of predominantly vertically aligned arrays with very small degree of tilting throughout the film. The analysis described above does not incorporate the possibility for more complex angle distribution functions. It restricts the distribution to a Gaussian shape in order to reduce the degrees of freedom during the optimization to only two parameters. Despite this simplification, the model captures most of the morphological aspects of the composites in a rigorous way. The general X-ray modeling protocol detailed in this section can be readily extended to other thin film systems to extract information regarding the long-range orientational order of mesoscale structures.

CONCLUSIONS

In this study a simple method to obtain vertically aligned arrays of nanorods in polymer thin films was developed. Furthermore, it was demonstrated that the interaction between nanorods is a dominant factor in the self-assembly process, and strong interactions in the case of alkyl-passivated nanocrystals result in the formation of macrophase separated arrays of nanorods with a high degree of orientational order. Also, the relatively weak polymer−nanorod interactions are responsible for the polymer-independent formation of nanorod arrays, making it possible to incorporate polymers with multiple functionalities and achieve engineered materials for a wide variety of applications. GISAXS experiments and models developed within this study allowed for a quantitative structural characterization of the nanorod−polymer composites and demonstrated the predominant vertical alignment of the nanorods over large areas (>1 cm^2). It also was demonstrated that kinetic effects are important in the self-assembly process, which lead to trapping of the nanorod arrays during film casting process and suggested a nanorod self-assembly process in solution. Further fundamental studies on the polymer mediated nanorod self-assembly in solution can enable control over the size of arrays and optimization of the nanocrystals−polymer interface for different applications. The general method described in this work can be used to fabricate nanostructured hybrid materials with potential to harness the anisotropic properties of nanorods for applications in photovoltaics, solar concentrators, polarized edge-emitters, and solar fuels membranes.

ASSOCIATED CONTENT

Supporting Information. SAXS results from concentrated solutions of nanorods and polymers and calculations on peak splitting arising from nanorod tilting. This material is available free of charge via the Internet at http://pubs.acs.org.

AUTHOR INFORMATION

Corresponding Author
*E-mail: segalman@berkeley.edu.

ACKNOWLEDGMENT

This work was funded by the Helios Solar Energy Research Center, which is supported by the Director, Office of Science, Office of Basic Energy Sciences of the U.S. Department of Energy. M.A.M. gratefully acknowledges an Arkema Graduate Fellowship that partly supported this work. J.J.U. thanks funding from the Molecular Foundry. This work made use of facilities at the Molecular Foundry, at the Advanced Light Source, and the National Center for Electron Microscopy all user facilities supported by the Office of Science, Office of Basic Energy Sciences, of the U.S. Department of Energy (Contract DE-AC02-05CH11231). Additionally, we gratefully acknowledge the Alivisatos group, A. Widmer-Cooper, J. L. Rivest, B. W. Boudouris, and B. McCulloch for helpful discussions and use of equipment.

REFERENCES

(1) Huynh, W. U.; Dittmer, J. J.; Alivisatos, A. P. *Science* **2002**, *295* (5564), 2425–7.

(2) Rizzo, A.; Nobile, C.; Mazzeo, M.; De Giorgi, M.; Fiore, A.; Carbone, L.; Cingolani, R.; Manna, L.; Gigli, G. *ACS Nano* **2009**, *3* (6), 1506–12.

(3) Hikmet, R. A. M.; Chin, P. T. K.; Talapin, D. V.; Weller, H. *Adv. Mater.* **2005**, *12*, 1436–1439.

(4) Amirav, L.; Alivisatos, A. P. *J. Phys. Chem. Lett.* **2010**, *1*, 1051–1054.
(5) Gudiksen, M. S.; Maher, K. N.; Ouyang, L.; Park, H. *Nano Lett.* **2005**, *5* (11), 2257–61.
(6) Talapin, D. V.; Koeppe, R.; Gotzinger, S.; Kornowski, A.; Lupton, J. M.; Rogach, A. L.; Benson, O.; Feldmann, J.; Weller, H. *Nano Lett.* **2003**, *3* (12), 1677–1681.
(7) Luo, Y.; Wang, L. W. *ACS Nano* **2010**, *4* (1), 91–8.
(8) Steiner, D.; Dorfs, D.; Banin, U.; Della Sala, F.; Manna, L.; Millo, O. *Nano Lett.* **2008**, *8* (9), 2954–8.
(9) Gupta, S.; Zhang, Q.; Emrick, T.; Russell, T. P. *Nano Lett.* **2006**, *6* (9), 2066–9.
(10) Ryan, K. M.; Mastroianni, A.; Stancil, K. A.; Liu, H.; Alivisatos, A. P. *Nano Lett.* **2006**, *6* (7), 1479–82.
(11) Carbone, L.; Nobile, C.; De Giorgi, M.; Sala, F. D.; Morello, G.; Pompa, P.; Hytch, M.; Snoeck, E.; Fiore, A.; Franchini, I. R.; Nadasan, M.; Silvestre, A. F.; Chiodo, L.; Kudera, S.; Cingolani, R.; Krahne, R.; Manna, L. *Nano Lett.* **2007**, *7* (10), 2942–50.
(12) Ahmed, S.; Ryan, K. M. *Nano Lett.* **2007**, *7* (8), 2480–5.
(13) Talapin, D. V.; Shevchenko, E. V.; Murray, C. B.; Kornowski, A.; Forster, S.; Weller, H. *J. Am. Chem. Soc.* **2004**, *126* (40), 12984–8.
(14) Baranov, D.; Fiore, A.; van Huis, M.; Giannini, C.; Falqui, A.; Lafont, U.; Zandbergen, H.; Zanella, M.; Cingolani, R.; Manna, L. *Nano Lett.* **2010**, *10* (2), 743–9.
(15) Zhao, N.; Liu, K.; Greener, J.; Nie, Z.; Kumacheva, E. *Nano Lett.* **2009**, *9* (8), 3077–81.
(16) Baker, J. L.; Widmer-Cooper, A.; Toney, M. F.; Geissler, P. L.; Alivisatos, A. P. *Nano Lett.* **2010**, *10* (1), 195–201.
(17) Peng, Z. A.; Peng, X. *J. Am. Chem. Soc.* **2002**, *124* (13), 3343–53.
(18) Hexemer, A.; Bras, W.; Glossinger, J.; Schaible, E.; Gann, E.; Kirian, R.; MacDowell, A.; Church, M.; Rude, B.; Padmore, H. *J. Phys.: Conf. Ser.* **2010**, *247*, 012007.
(19) Titov, A. V.; Kral, P. *Nano Lett.* **2008**, *8* (11), 3605–12.
(20) Krishnan, R. S.; Mackay, M. E.; Duxbury, P. M.; Pastor, A.; Hawker, C. J.; Van Horn, B.; Asokan, S.; Wong, M. S. *Nano Lett.* **2007**, *7* (2), 484–9.
(21) Ploshnik, E.; Salant, A.; Banin, U.; Shenhar, R. *Adv. Mater.* **2010**.
(22) Son, D. I.; Park, D. H.; Choi, W. K.; Kim, T. W. *Nanotechnology* **2009**, *20* (27), 275205.
(23) Tolan, M. *Springer Tracts Mod. Phys.* **1999**, *148*, 116.
(24) Stein, G. E.; Kramer, E. J.; Li, X. F.; Wang, J. *Macromolecules* **2007**, *40* (7), 2453–2460.
(25) Renaud, G.; Lazzari, R.; Leroy, F. *Surf. Sci. Rep.* **2009**, *64* (8), 255–380.
(26) Sinha, S. K.; Sirota, E. B.; Garoff, S.; Stanley, H. B. *Phys. Rev. B* **1988**, *38* (4), 2297–2311.
(27) Parratt, L. G. *Phys. Rev.* **1954**, *95* (2), 359–369.
(28) Guinier, A.; Fournet, G. *Small-Angle Scattering of X-Rays*; John Wiley and Sons: New York, 1955.
(29) Smilgies, D. M. *J. Appl. Crystallogr.* **2009**, *42*, 1030–1034.